ACS Sustainable Chemistry & Engineering

Research Article

Cite This: ACS Sustainable Chem. Eng. 2018, 6, 668–678

pubs.acs.org/journal/ascecg

Understanding the Effect of the Dianhydride Structure on the Properties of Semiaromatic Polyimides Containing a Biobased Fatty Diamine

Arijana Susa,* Johan Bijleveld, Marianella Hernandez Santana,† and Santiago J. Garcia

Novel Aerospace Materials Group, Faculty of Aerospace Engineering, Delft University of Technology, Kluyverweg 1, 2629 HS, Delft, The Netherlands

Supporting Information

ABSTRACT: In this work we report the effect of the hard block dianhydride structure on the overall properties of partially biobased semiaromatic polyimides. For the study, four polyimides were synthesized using aliphatic fatty dimer diamine (DD1) as the soft block and four different commercially available aromatic dianhydrides as the hard block: 4,4′-(4,4′-isopropylidenediphenoxy) bis(phthalic anhydride) (BPADA), 4,4′-oxidiphthalic anhydride (ODPA), 4,4′-(Hexafluoroisopropylidene) diphthalic anhydride (6FDA), and 3,3′,4,4′-biphenyltetracarboxylic dianhydride (BPDA). The polymers synthesized were fully organosoluble thermoplastic branched polyimides with glass transition temperatures close to room temperature. The detailed analysis took into account several aspects of the dianhydrides structure (planarity, rigidity, bridging group between the phtalimides, and electronic properties) and related them to the results obtained by differential scanning calorimetry, rheology, fluorescence and broadband dielectric spectroscopy. Moreover, the effects of physical parameters (crystallization and electronic interactions) on the relaxation behavior are discussed. Despite the presence of the bulky branched soft block given by the dimer diamine, all polyimides showed intermolecular charge transfer complexes, whose extent depends on the electronic properties of the dianhydride hard block. Furthermore, the results showed that polyimides containing flexible and bulky hard blocks turned out fully amorphous while the more rigid dianhydride (BPDA) led to a nanophase separated morphology with low degree of crystallinity resulting in constrained segmental relaxation with high effect on its mechanical response with the annealing time. This work represents the first detailed report on the development and characterization of polyimides based on a biobased fatty dimer diamine. The results highlight the potential of polymer property design by controlled engineering of the aromatic dianhydride blocks.

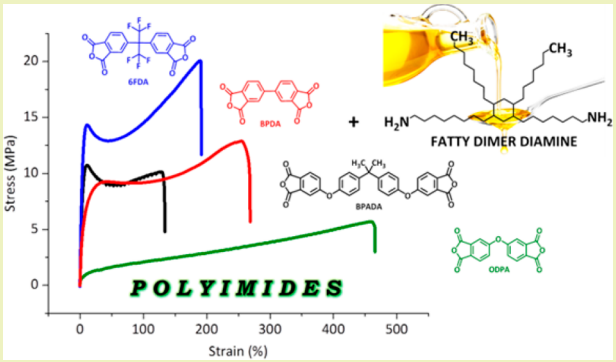

KEYWORDS: *Polyimides, Fatty dimer diamine, Alkyl branches, Aromatic dianhydrides, Structure–polymer properties*

INTRODUCTION

Due to increased concerns regarding environmental sustainability, highly directed by growing and demanding ecological regulations, renewable resources are increasingly receiving both industrial and academic attention.[1−3] Among the different renewable sources vegetable oils are generally considered the most important class due to their availability and versatility. Vegetable oils are used to synthesize different types of polymers[4] such as polycarbonates, polyurethanes, polyesters, polyethers, polyamides, and polyolefins[5] for paints, adhesives, composites, and biomedical applications.[3] Various thermoset and thermoplastic polymers can be obtained, resulting in miscellaneous characteristics to meet many different industrial requirements, thereby confirming vegetable-oil based polymers' potential as alternatives to petroleum-based ones.[6,7]

Vegetable oils are composed of different triglycerides which are the esterification products of glycerol with various fatty acids. The heterogeneity and variability of the triglycerides, which is due to the statistical distribution of fatty acids per triglyceride, makes a clear and reproducible correlation between the material properties and the monomer structures difficult. However, utilizing difunctional fatty acid-based monomers (diols, diamines, and diacids) with a well-defined molecular structure can lead to biobased polymers with better tunable properties.[8] Fatty dimers have been used in the past to prepare polymers with innovative molecular architectures, such as supramolecular polymers with hydrogen bonding[9] or reversible ionic interactions[10] and PU–acrylate coatings.[11] They are reportedly being utilized for suppressing H-bonding, inducing phase segregation and tuning viscosity, crystallinity, and thermo-mechanical properties in renewable polyurethanes and polyamides[12,13] and their biocomposites.[14,15] More recently

Received: August 30, 2017
Revised: November 13, 2017
Published: November 30, 2017

DOI: 10.1021/acssuschemeng.7b03026
ACS Sustainable Chem. Eng. 2018, 6, 668–678

Scheme 1. Structures of the Monomers Used in the Polyimides Synthesis[a]

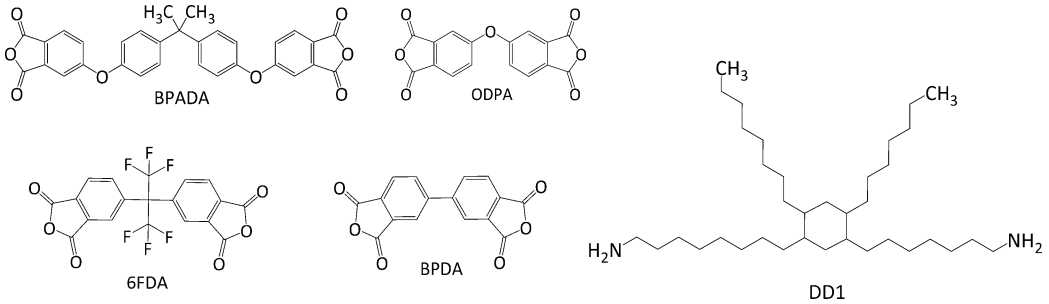

[a]The left side shows four dianhydrides used (BPADA, ODPA, 6FDA, and BPDA) and the right side shows a generalized structure of the dimer diamine (DD1).

Scheme 2. Schematic Representation of the Thermal Imidization Reaction (Cyclodehydration of Polyamic Acid into a Polyimide)

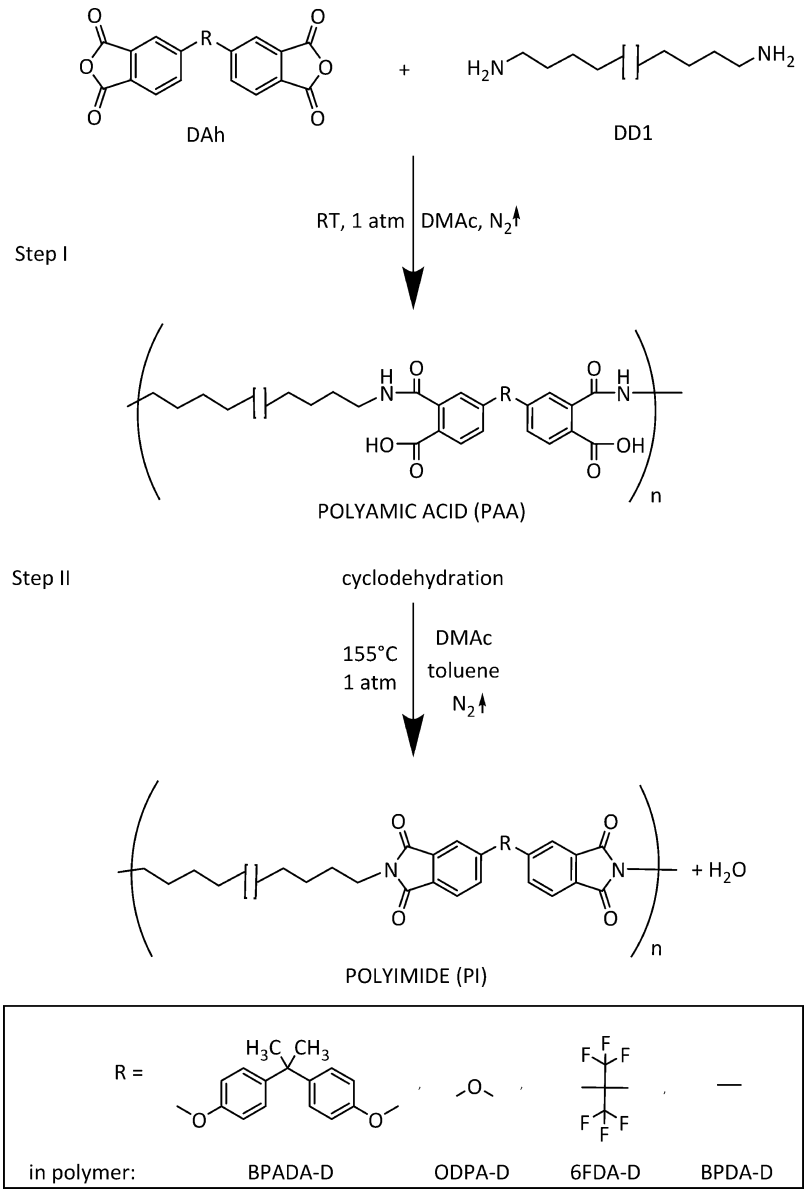

biobased fatty dimer diamines with long alkyl branches (Priamine) were reported as useful building blocks to develop room temperature self-healing polyimides with high mechanical properties.[16,17] In that previous work we reported[16] the effect of the stoichiometric offset of the ODPA/DD1 ratio on the dynamic mechanical and self-healing properties of the resulting polymers. However, the role of the dianhydride architecture on the overall properties of these fatty dimer diamine based

DOI: 10.1021/acssuschemeng.7b03026
ACS Sustainable Chem. Eng. 2018, 6, 668−678

polyimides was not examined, leaving room for further dedicated research.

Polyimides are known for their capability of forming intra- and interchain electronic interactions called charge-transfer complexes (CTC), which are the reason behind their high thermo-mechanical properties and deep coloration.[18] However, most of the aromatic polyimides are insoluble in any organic solvent. That, in addition to very high transition temperatures, often higher than their decomposition temperatures, limits their usefulness for many applications.[19] Flexible and bulky linkage groups are traditionally being introduced between aromatic rings in the dianhydride monomer[20,21] to enhance solubility, transparency, and processing. The goal of these modifications is to either disrupt their aromaticity (to prevent intramolecular conjugation) or to make the chains pack less efficiently (to prevent intermolecular CTC formation). Naturally, modification of the molecular architecture of PIs influences their mechanical properties and molecular dynamics as well.[22−24]

In this work we report the effect of the aromatic dianhydride structure on the thermal, optical, and mechanical properties and relaxation behavior of a set of polyimides based on a biobased aliphatic dimer diamine (DD1). The results are discretized with regards to several aspects: planarity, rigidity, bridging group between the phtalimides, electronic properties, and the combinations thereof. Moreover, the effect of different physical constraints (crystal formation and electronic interactions) on the relaxation behavior is discussed in detail. Despite their partially aliphatic and densely branched architectures, it was found that the synthesized polyimides are still able to form intermolecular charge transfer complexes, playing an important role in the overall properties of these semiaromatic thermoplastic polyimides. To the best of our knowledge, this is the first time that the effect of fatty dimer diamine is explored in a set of different polyimides with varying dianhydride architecture.

EXPERIMENTAL SECTION

Synthesis. Four aromatic dianhydrides were used as hard aromatic block (Scheme 1): 4,4′-(4,4′-isopropylidenediphenoxy) bis(phthalic anhydride) (BPADA; 97%, Sigma-Aldrich), 4,4′-oxidiphthalic anhydride (ODPA; 98%, TCI Europe N.V.), 4,4′-(hexafluoroisopropylidene) diphthalic anhydride (6FDA; 98%, TCI Europe N.V.), 3,3′,4,4′-biphenyltetracarboxylic dianhydride (BPDA; 98%, TCI Europe N.V.). The soft block was in all cases a fatty dimer diamine derived from vegetable oil (Priamine 1075, here named DD1; Croda Nederland B.V.) with the structure as shown in Scheme 1. DD1 appears as a light yellow viscous liquid with melting point at −30°C and 100% renewable carbon content. Theoretical stoichiometric ratios, calculated according to the molecular weights of the monomers (MW_{BPADA} = 520.49 g/mol, MW_{ODPA} = 310.20 g/mol, MW_{6FDA} = 444.24 g/mol, MW_{BPDA} = 294.22 g/mol, and MW_{DD1} = 536.80 g/mol) and assuming all chemicals are 100% difunctional, were used. The synthesis was conducted in *N*,*N*-dimethylacetamide (DMAc, 99.5% extra dry, Acros Organics) polar aprotic solvent with total solids (monomers) content of 20 wt %. Using a two-step polymerization process as described in Scheme 2, four polymers were obtained: BPADA-D, ODPA-D, 6FDA-D, and BPDA-D. The details of the synthesis procedure in Scheme 2 can be found elsewhere.[16]

Characterization Methods. *Infrared Spectroscopy.* Attenuated total reflectance Fourier transform infrared (ATR-FTIR) spectroscopy was employed in order to follow reaction completion. Each IR spectrum was recorded as an average of two scans in the wavenumber range 4000−500 cm^{-1}.

Gel Permeation Chromatography (GPC). Molecular weight distributions of synthesized polymers were determined by GPC on a Shimadzu Prominence GPC system equipped with a Shodex LF-804 column and a refractive index detector. The flow rate of the eluent tetrahydrofuran (THF) was 1 mL/min, and polystyrene was used as the standard. Polymer solutions were prepared in THF at 1 mg/mL and the samples were filtered (0.45 μm syringe filter) prior to use.

Thermal Analysis. Thermal properties were evaluated by PerkinElmer Pyris Diamond TG/DTA thermogravimetric analysis (TGA) and PerkinElmer Sapphire differential scanning calorimetry (DSC). All measurements were performed under nitrogen. TGA was run from room temperature to 500 °C at 10 °C/min. DSC measurements were carried out at 10 °C/min following this procedure: (1) heating from −50 to +200 °C; (2) holding at 200 °C for 2 min; (3) cooling to −50 °C, and (4) repeat steps 1 to 3. The glass transition temperature (T_g) was determined from the second heating cycle.

Density Determination. The density of the polymers was determined by hydrostatic weighing method coupled with an analytical laboratory scale with a precision of 0.1 mg.

Rheological Measurements. The linear viscoelastic properties of the PIs were investigated by the Haake Mars III rheometer, using the parallel plate geometry, with plate diameter of 8 mm. Preliminary strain amplitude sweeps at 1 Hz were performed at the highest and the lowest tested temperatures, from 0.001% to 10% strain to evaluate the extension of the linear viscoelastic region for the different polymers. Based on these results, a shear strain of 0.5% for all polymers was used to ensure the tests were performed in the linear viscoelastic region. Temperature sweep experiments were performed at 1 Hz in a cooling ramp from 50 to 5 °C. The tan δ curves from the temperatures sweeps were used to determine T_g from the maximum of the tan δ peak ($T_g = T(\tan \delta_{MAX})$). For the aim of activation energies, E_a, calculations, the frequency sweep experiments from 10 to 0.1 Hz were performed at temperatures between 110 and 10 °C, in steps of 5 °C. Tests were repeated twice-showing high reproducibility. The rheological master-curves at the reference temperature of the previously determined $T_g = T(\tan \delta_{MAX}) = T_{ref}$ were constructed from the obtained data applying the time−temperature superposition principle (TTS) using the dedicated Rheowin software. From the shift factors, a_T, the Arrhenius plots ($\ln a_T$ vs $1000/T$) were constructed and the activation energies were calculated from the slopes of the linear fit,[25] as shown in the Supporting Information (S-6).

Broadband Dielectric Spectroscopy (BDS). BDS measurements were performed on an ALPHA high resolution dielectric analyzer (Novocontrol Technologies GmbH). All samples were mounted in the dielectric cell between two parallel gold-plated electrodes. The complex permittivity $\varepsilon^*(\omega) = \varepsilon'(\omega) - i\varepsilon''(\omega)$ of each sample was measured by performing consecutive isothermal frequency sweeps over a frequency window of $10^{-1} < f\,(\mathrm{Hz}) < 10^6$ (where $f = w/2\pi$ is the frequency of the applied electric field) in the temperature range from 0 to 100 °C in steps of 5 °C. The resulting relative error of each parameter is less than 3%.

Tensile Properties. Tensile mechanical tests were performed on an Instron model 3365 universal testing systems equipped with a 1 kN load cell, using dog-bone specimens according to the ASTM D1708 standard (thickness, $t = 2 \pm 0.5$ mm) at 80 mm/min crosshead speed and ambient temperature (23 ± 2 °C).

Fluorescence Spectroscopy. The fluorescence spectra of polyimides were obtained using a PTI QuantaMaster Photoluminescence Spectrometer equipped with 75 W Xe lamp and using a PMT voltage of 1000 V. The same specimen geometry as for the tensile test was used. First the excitation scan was run in the range 280−400 nm, collecting emission at 410 nm. From this, the fluorescent peak was determined at 360 nm. Further, the samples were excited at that particular wavelength and monitored over the range 370−700 nm using an aperture slit width of 2 nm with 1 nm step size and 0.1 s integration time during monitoring. Each measurement was repeated three times, showing good reproducibility. The sample thickness was found not to have an effect on the measured peak.

RESULTS AND DISCUSSION

Effect of the Dianhydride Structure on the PIs Properties. The imidization of PAA into PI can be confirmed

DOI: 10.1021/acssuschemeng.7b03026
ACS Sustainable Chem. Eng. 2018, 6, 668−678

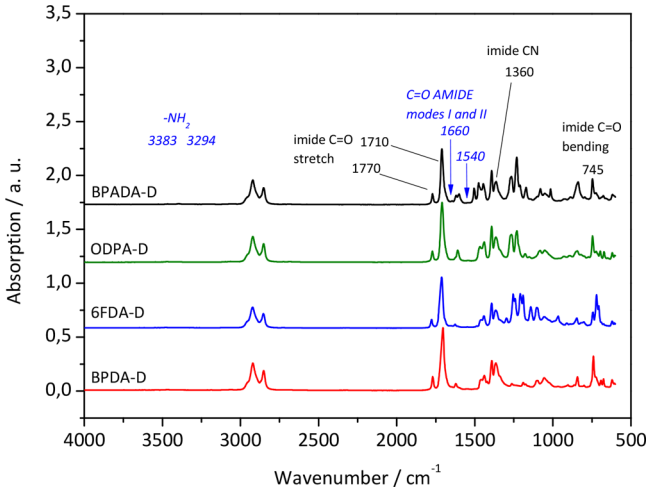

Figure 1. IR spectra of four PIs with different dianhydrides showing characteristic imide peaks (labeled black) and absence of prepolymer (amide) peaks (labeled italic blue).

by IR spectroscopy using the disappearance of the amic acid peaks typically visible at 1716, 1640, and 1550 cm^{-1} in PAA spectra and the appearance of the characteristic peaks of imide bonds at 1770, 1710, 1360, and 745 cm^{-1} in PI spectra. The imidization reaction was confirmed for all of the polymers (Figure 1) and supported by ^1H NMR analysis (Figure S1, Supporting Information). The percentage yields were calculated by the standard approach shown in the SI (Page S-2). Yields of 83% for BPADA-D, 89% for ODPA-D, 74% for 6FDA-D, and 73% for BPDA-D were obtained.

As can be seen from the TGA curves (Figure S2, Supporting Information), all polymers show a high thermal stability independent of the dianhydride architecture with values for the onset degradation temperature (2% weight loss) at 330–380 °C (Table 1) similar to those of traditional commercial polyimides such as LaRC-IA. All samples showed only a small weight loss up to 0.6% until 200 °C suggesting that almost no solvent (toluene or DMAc) was entrapped during the imidization and that the monomers were fully reacted. The resulting polymers were fully soluble in common organic solvents, such as toluene, THF, and chloroform, which facilitates their processing (for example, in coatings, adhesives and thin films applications), as opposed to commercial polyimides.[19] The GPC results are presented in Table 1. The small differences in the molecular weights might be due to various reasons, such as impurities or side-reactions but also differences in the electron affinities of the aromatic dianhydrides. As the susceptibility of the nucleophilic attack increases with the electrophilicity of the dianhydride group, the reactivity of the dianhydride monomer is related to its electron affinity: higher values indicate higher reactivity of the dianhydride. According to the literature,[18,26] the electron affinities of the dianhydrides used in this work increase in the order BPADA-D < ODPA-D < BPDA-D < 6FDA-D.

The flexibility of the dianhydride moieties is reflected in the value of the T_g, where three polymers (BPADA-D, 6FDA-D, and BPDA-D) exhibit a similar T_g, ranging from 22 to 25 °C and ODPA-D showing a lower value of 13 °C. The T_g values of these PIs are incomparable to those of fully aromatic commercial PIs ($200 < T_g < 400$ °C),[27] which naturally excludes the possibility for their use in high-temperature applications. However, their T_g's are higher than the ones of other reported polymers that contain fatty acid dimer as the building block that remained significantly below room temperature. The ionic supramolecular networks prepared from fatty acid dimer by Aboudzadeh et al. exhibit their T_g's in the range $-29 < T_g < 10$ °C.[10] The fatty acid dimer based polyamides from Hablot at al. showed $-17 < T_g < -5$ °C,[12] while the values in the range $-10 < T_g < -0.9$ °C were obtained in the fatty acid dimer based polyamides synthesized by van Velthoven et al.[13]

The ODPA and BPADA dianhydrides have a very flexible oxygen linker between the two phtalic anhydride parts of the molecule (Scheme 1). Comprising two oxygen linkers, BPADA may appear the most flexible out of the four dianhydrides used here, yet it does not exhibit the lowest T_g. This is likely to be caused by the increase in aromatic content compared to ODPA-D, where the extra flexibility of the ether linkage is counterbalanced by the increased number of aromatic rings. Despite the structural differences, BPDA-D and 6FDA-D display a similar T_g. The expected increase in backbone flexibility of the 6FDA-D polymer may be compensated by the extra bulkiness of the CF_3 groups. A similar effect of dianhydride structure on the T_g of nonbranched fully[20] and partially aromatic[28] polyimides was reported in the literature, with the exception of BPADA. A detailed DSC analysis (Figure S3, Supporting Information) shows the absence of melting or crystallization peaks thereby reflecting the amorphous nature of all of the polyimides in their state just after synthesis.

Rheological temperature sweeps were performed at a very slow cooling rate (1 °C/min), and the results are shown in Figure 2. Figure 2a shows the values of the storage modulus (G') and loss modulus (G'') while damping factors (tan δ) versus temperature at 1 Hz for all of the samples studied are shown in Figure 2b.

The differences between the T_g values determined from the maximum of the tan δ peak (25 °C < T_g < 40 °C) arise from

Table 1. Effect of the DAh type on Mw, Mn, and PDI as Calculated from the Major Peak Obtained in GPC[a]

polymer	Mw (g/mol)	Mn (g/mol)	PDI	DSC-T_g (°C)	rheology-T_g (°C)	BDS-T_g[d] (°C)	TGA T (2% weight loss) (°C)	density (g/cm^3)
BPADA-D	29k	18k	1.6	24	36	20	360	1.05
ODPA-D	32k	16k	2.0	13	25	11	380	1.05
6FDA-D	41k	20k	2.0	25	40	21	330	1.12
BPDA-D	37k	20k	1.9	22	33[e], 46[e]	18	350	1.05

[a] T_g obtained from DSC, rheology, and BDS and temperatures for 2% weight loss obtained from TGA. Samples were tested as produced. [b] T_g was calculated from the 2nd heating curve, 10 °C/min. [c] T_g was taken as the maximum of the peak in the tan δ curve from the temperature sweeps, performed in cooling ramp, 1 °C/min. [d] T_g is obtained from the broadband dielectric spectroscopy (BDS) measurements, by extrapolating the VFT fit to the temperature at which τ_{max} is equal to 100 s (see Figure S5, Supporting Information). [e] Polymer BPDA-D exhibits two T_g peaks [T_g (I) and T_g (II)] in rheological temperature sweep plots, which is shown and discussed later in the article.

DOI: 10.1021/acssuschemeng.7b03026
ACS Sustainable Chem. Eng. 2018, 6, 668–678

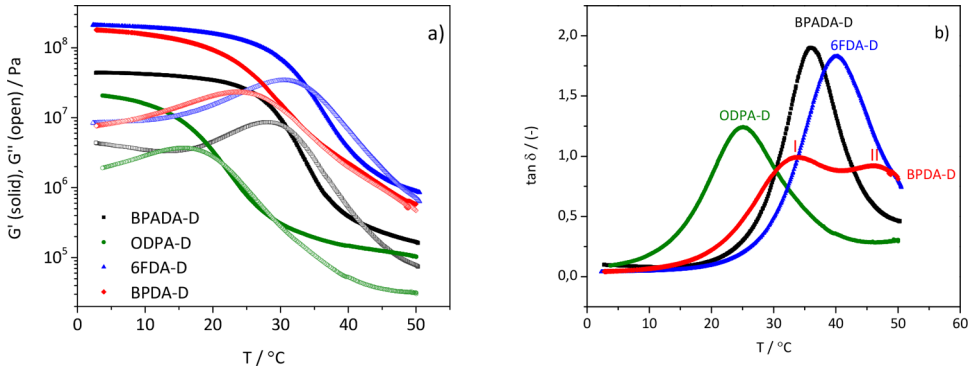

Figure 2. (a) Storage (G') and loss (G'') moduli and (b) tan δ curves from the rheological temperature sweeps experiments, showing distinct T_g relaxations of the four PIs.

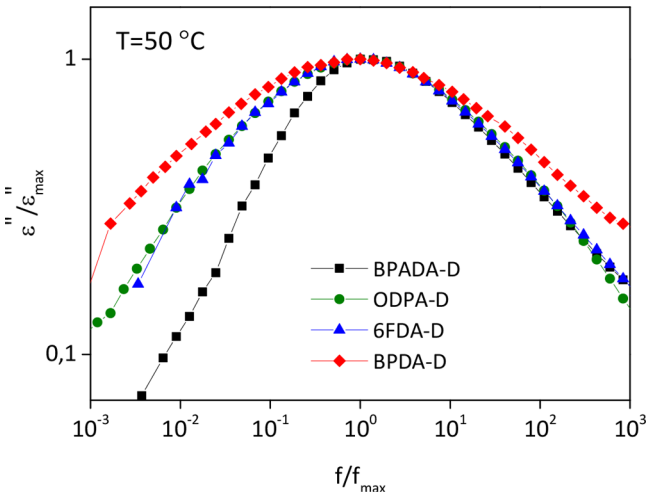

Figure 3. Normalized dielectric loss log(ε'') vs normalized frequency log(f) of PI samples with different dianhydrides at T = 50 °C.

the effect of different aromatic dianhydride structures on the glass transition processes. The width of the curves indicate the breadth of the temperature range over which the glass transition occurs but also the polymer structural heterogeneity.[29] The values of tan δ of these polymers (especially BPADA-D and 6FDA-D with values close to 2) are remarkably high over a broad range of near-room temperatures, which makes them great candidates in applications where high damping properties are required at ambiental conditions (noise or vibration insulating materials, shock absorbers, and sealants). In general, damping materials with tan δ>0.5 are considered for outdoor or machinery applications.[30] (As seen in Figure 2b, BPADA-D and 6FDA-D are displaying the narrowest tan δ peaks. A somewhat broader curve was obtained with ODPA-D and the broadest with BPDA-D. Moreover, the BPDA-D system exhibits stepwise glass transition (shown in Figure 2b as (I) and (II)), as opposed to the other three (BPADA-D, ODPA-D, and 6FDA-D), which show single T_g.

Similar observations could be made from the broadband dielectric spectroscopy (BDS) data. The spectra corresponding to all four polymers over a wide range of frequencies at different temperatures are shown in Figure S4, Supporting Information. T_g was calculated from the temperature dependence of the segmental relaxation times (τ_{max}). When this dependence follows a Vogel–Fulcher–Tammann (VFT) behavior, T_g is obtained by extrapolating the VFT fit to the temperature at which τ_{max} is equal to 100 s (see the SI).[31] The T_g's calculated following this approach (Table 1) are similar to the values obtained by DSC and follow the same trend of increase among the four polymers investigated (ODPA-D < BPDA-D < BPADA-D < 6FDA-D), as seen by DSC and rheology. The temperature dependence of the relaxation times in the whole region of the segmental relaxation further supports the fact that the ODPA-D polymer has the least restricted dynamics (see the SI).

In addition to a third estimate of T_g, BDS gave some further insights on the structure and polymer architecture of the studied PIs.

By plotting the normalized dielectric loss vs normalized frequency, a clearer view on how the shape (symmetry and broadness) of the relaxation spectra varies is obtained. Figure 3 shows the normalized plots at a selected temperature (T = 50 °C) at which the dielectric relaxation is clearly observable as a well-resolved peak in the frequency window for all polymers. Depending on the nature of the dianhydride incorporated into the polymer, clear differences in the shape of the spectra can be noticed. Schönhals and Schlosser[32] phenomenological model proposes that the shape of the normalized dielectric loss peak is related to the behavior of the polymer at low and high frequencies, controlled by inter- and intramolecular interactions, respectively. The application of such a model to the studied polyimides suggests that the differences on the low frequency side may be related to the changes in the dynamics of the main chain segments due to the contribution/restriction imposed by the different dianhydrides, while the variations on the high frequency side can be attributed to the influence of the dangling side chains.

In order to quantify these differences, the dielectric strength ($\Delta\varepsilon$) and the shape parameters b and c derived from the Havriliak–Negami (HN) fitting function (see the SI) were calculated and shown in Figure 4. The b and c parameters characterize the symmetric and asymmetric broadening of the relaxation time distribution, respectively. The term $b*c$ is also shown in the same figure. In a log(ε'') vs log(f) plot, just as in Figure 3, the shape parameters b and $b*c$ correspond to the low- and high-frequency slopes of the relaxation function respectively, with regards to the position of the maximal loss.[33]

A detailed analysis of the plots in Figure 4 gives better insight into the effect of different dianhydrides on the resulting polymer architectures. An increase in dielectric strength ($\Delta\varepsilon$) can be understood in terms of an increasing number of mobile dipoles (increasing fraction of polar molecules) involved in the relaxation, indirectly reflecting stronger molecular interactions.

DOI: 10.1021/acssuschemeng.7b03026
ACS Sustainable Chem. Eng. 2018, 6, 668–678

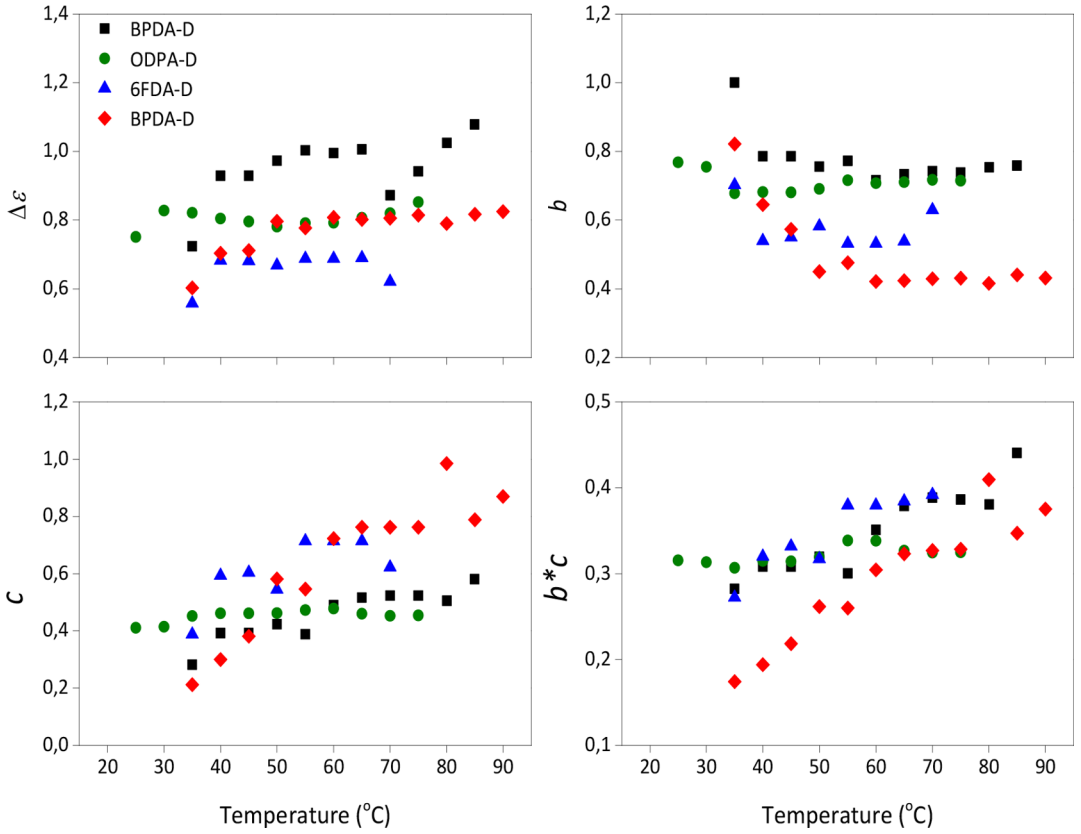

Figure 4. Dielectric parameters derived from the HN fitting function in the temperature range of the segmental relaxation.

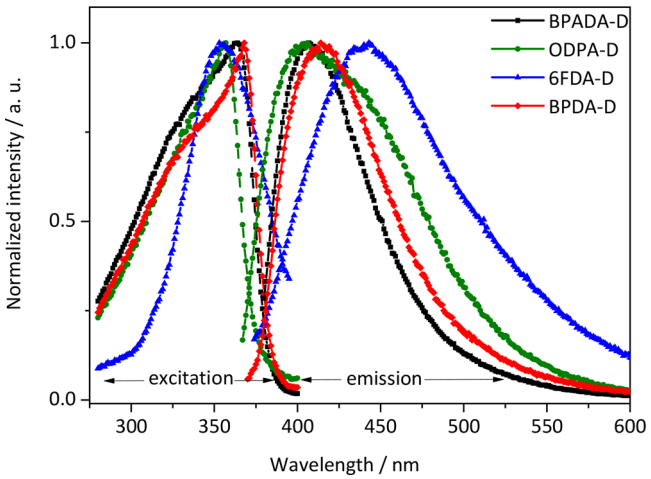

Figure 5. Optical properties of the four PIs: fluorescence excitation (left) and emission (right) spectra, normalized by maximum. λ_{exc} = 360 nm.

Table 2. Annealing Temperatures Taken as Maxima of the tan δ Peak (T_g) of the Rheological Temperature Sweep Curves (Figure 2b)

polymer	$T_{ann} = T(\tan \delta_{MAX}) = T_g$/°C
BPADA-D	36
ODPA-D	25
6FDA-D	40
BPDA-D	33

We can therefore infer that the BPADA-D system has higher dipole interactions than the rest of the PI systems with other dianhydrides. Recently, research on the relaxation behavior of thermo-reversible elastomer networks based on 2-ureido-4-pyrimidinone (UPy) dimers has been published by Luo et al.[34] In their work they report on the appearance of a new relaxation, seen as a shoulder close to the segmental relaxation, ascribed to the dissociation dynamics of dimer complexes within the network. They conclude that this new relaxation is related to the local UPy dimers dynamics resulting from the dissociation and reformation of the complexes. They also report an increase of $\Delta\varepsilon$ due to the increased number of dissociated UPy units. In our work, there is no evidence of a new relaxation probably because they take place within the temperature range within the glass transition; therefore, any weaker relaxation is hidden by the strong segmental relaxation.

Second, the fact that the b parameter is higher for the BPADA-D system reflects a narrower and more symmetrical loss peak. In terms of the polymer architecture, this would suggest a more homogeneous structure formed by polymer chains with similar large scale motions. On the contrary, the lowest b value for the BPDA-D system suggests chain segments with different dynamics and thus a higher degree of structural heterogeneity, implying regions of distinct mobility. This hypothesis is confirmed by the presence of a stepwise glass transition, as reported by rheological measurements (Figure 2b). Moreover, the lowest $b*c$ parameter for BPDA-D is further confirming heterogeneous dynamics of this sample with a more visible temperature dependence. As the temperature increases, the $b*c$ parameter tends to increase, presuming the distinct heterogeneous mobility regions become more homogeneous, especially above 50 °C. As will be discussed later on, the increase on $b*c$ values above 50 °C could be related to local

DOI: 10.1021/acssuschemeng.7b03026
ACS Sustainable Chem. Eng. 2018, 6, 668−678

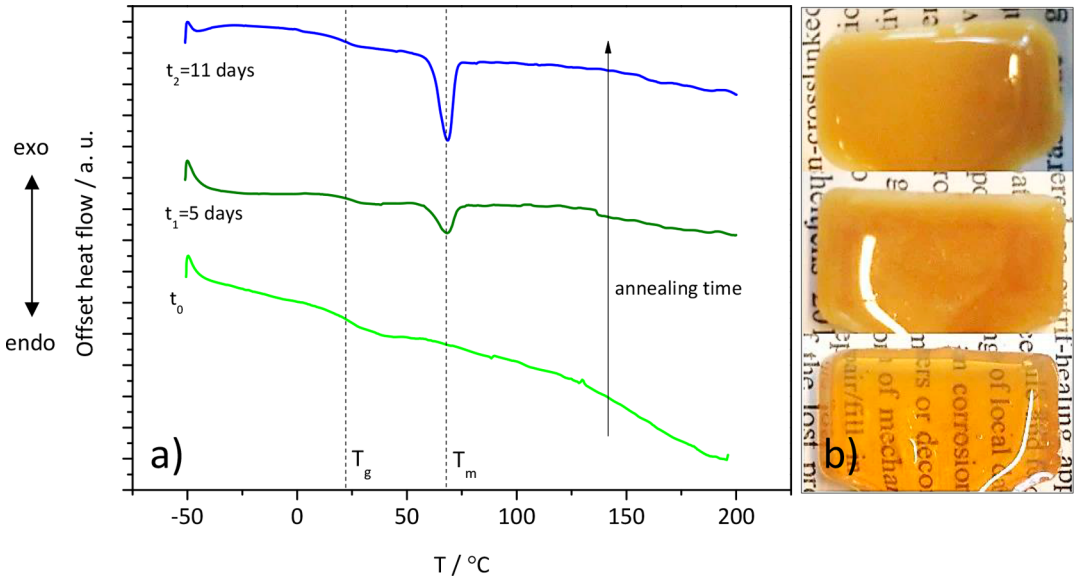

Figure 6. (a) DSC traces from the second heating curve with T_g and T_m indicated by the dashed lines and (b) corresponding images showing increase in opacity of BPDA-D polymer with annealing time. $T_{ann} = T(\tan \delta_{MAX}) = T_g$.

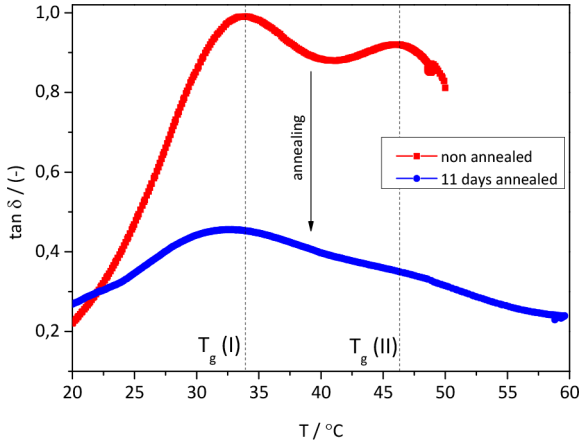

Figure 7. Rheological T-sweep curves. Effect of annealing on the glass transition relaxation behavior of the BPDA-D polymer. Red curve represents the nonannealed polymer and the blue curve shows the polymer annealed for 11 days at $T_{ann} = T(\tan \delta_{MAX}) = T_g$.

ordering present in the BPDA-D sample appearing at around 50 °C.

Aromatic polyimides are well-known for forming charge transfer complexes (CTCs), which are widely claimed to be the reason behind their great mechanical and thermal properties, as well as their characteristic colors,[18] due to their absorption characteristics tailings in the visible region caused by the intra and/or intermolecular charge transfer (CT) interactions of the PI backbones. Moreover, CTCs have a major effect on the chain packing.[27,35] In order to investigate the origin of the different coloration, the polymer optical properties were tested by fluorescence spectroscopy as typically used in polyimide research to identify the formation of CTCs.[18,35−39] The CTCs existence has been previously confirmed for not only fully aromatic PIs but also in the semiaromatic ones.[40] Our results showed that CTCs in the branched polyimides are identified by a long-wavelength absorption at $\lambda > 330$ nm, similar to those reported in literature.[37,38] As can be seen in Figure 5, the four polyimides developed in this work are fluorescent in the CTC-region (400 nm < λ_{em} < 450 nm).

Effect of the Low Temperature Annealing on Local Ordering. Another important factor affecting the physical properties of polyimides is the aggregation state of polymer chains, i.e., macromolecular packing. Many have shown that imidization temperature affects the aggregation state of PIs,[38] but the postimidization thermal treatment (i.e., annealing) does as well.[41] In order to further explore the origin of physical constraints on the properties of the given set of DD1 based PIs, they were subjected to low temperature annealing, $T_{ann} = T(\tan \delta_{MAX}) = T_g$ (see Table 2), for 1, 5, and 11 days. Their thermal, optical, and mechanical properties were then evaluated as a function of the annealing time. The DSC scans of all four polymers show no change in their T_g values.

However, as opposed to the other three polymers, a change in opacity with time was noticed for BPDA-D, turning from translucent to fully turbid after 5 and 11 days at T_{ann}. DSC scans of turbid BPDA-D show an appearance of a melting peak at 68 °C (yet no change in the T_g value). The melt enthalpy increases from 5 J/g (for 5 days annealed) to 11 J/g (for 11 days annealed) with no change in T_m (Figure 6). As seen by polarized microscopy (Figure S7, Supporting Information), the birefringence increases with annealing time as well. These observations can be explained by the rigidity and planarity of the BPDA monomer which result in the chain regularity and hence efficient chain packing, allowing the BPDA-D polymer to crystallize.[28] At this stage it is not possible to unambiguously state which segments of the molecule crystallize. Nevertheless, the increase of order in chain packing with annealing time in BPDA-D polymer was confirmed by small-angle X-ray scattering measurements, SAXS (Figure S8, Supporting Information) by the appearance of two additional peaks at annealing times 5 and 11 days, with respect to 1 day. The peak ratio is q_1:q_2:q_3 = 1:2:3, which was previously reported to be related to the nanophase separation in lamellar morphology.[42] Taking in account that T_m is rather low (68 °C) and considering reported similar range of T_m values for other partially aromatic polymers with alkyl side branches in the literature,[43,44] we suggest that crystals might be formed within

DOI: 10.1021/acssuschemeng.7b03026
ACS Sustainable Chem. Eng. 2018, 6, 668−678

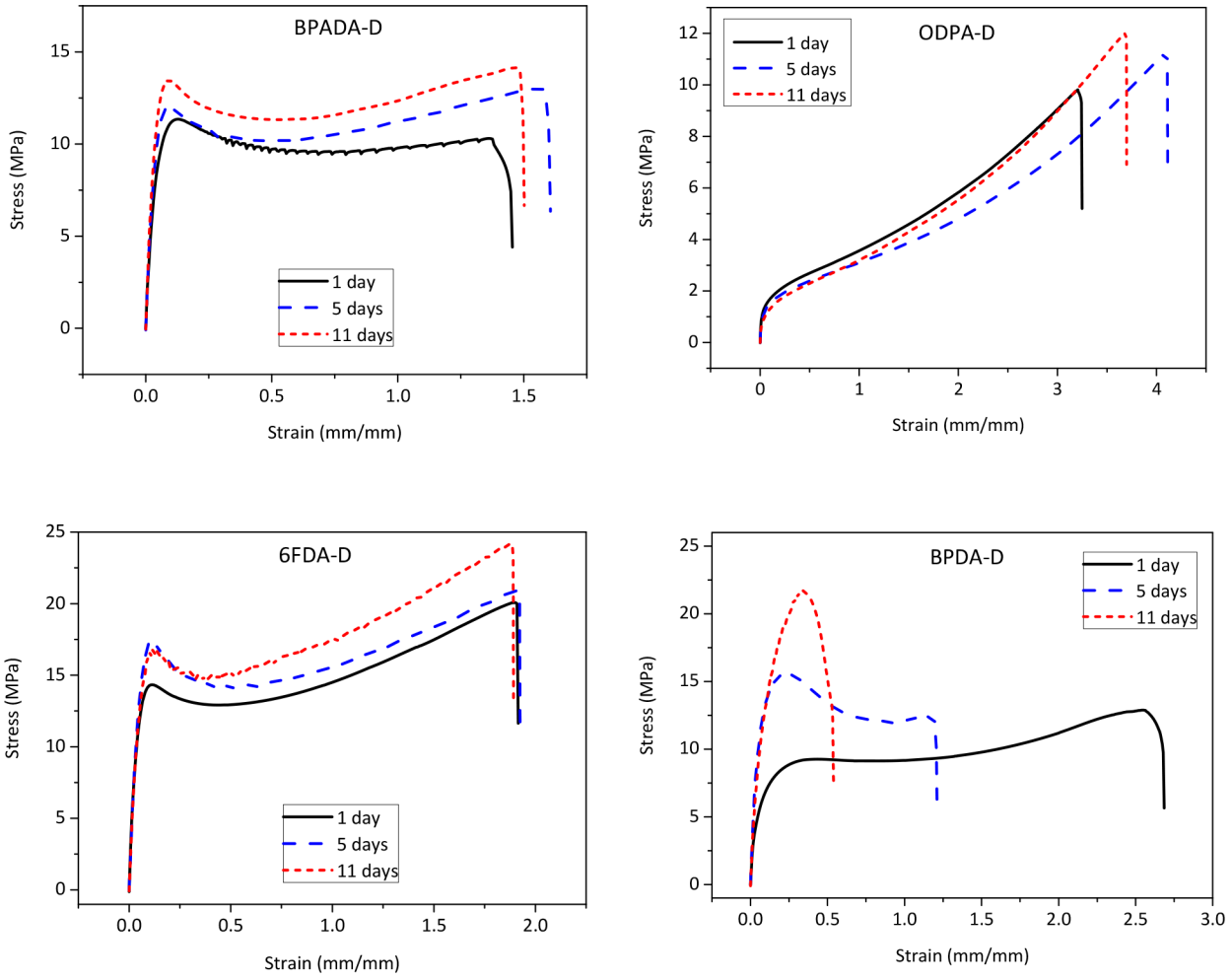

Figure 8. Effect of annealing time on the stress−strain behavior of the four PIs. $T_{ann} = T(\tan \delta_{MAX}) = T_g$.

the nanodomains of the alkyl side branches. As Beiner and Huth suggested, this may be a result of a confinement of the alkyl side chains by less-mobile main chains.[45] However, further research is necessary to confirm this hypothesis.

On the contrary, the polymers with the other three dianhydrides remain fully amorphous with the annealing time. Even though rigid, the bulky hexafluoroisopropylidene spacer of 6FDA dianhydride causes distortions of backbone symmetry which prevents the parallel alignment of the chains. On the other hand, the ether linkages of BPADA and ODPA are not bulky but offer high rotational freedom and flexibility which reduces the rigidity of the backbone, introduces kinks which hinder the coplanarity and thus prevent any efficient chain packing.[22,27,28] The same dianhydride effect on crystallization ability was noticed in fully aromatic rigid rod polyimides and copolyimides, comprising various diamines. For example, Arnold et al. prepared nine polyimides using six different dianhydrides, including ODPA, 6FDA, and BPDA among others. Only two polymers with different diamines were able to crystallize during drawing or/and annealing and both of them comprised BPDA as the dianhydride.[46]

While the rheological temperature sweeps of the polymers BPADA-D, ODPA-D, and 6FDA-D do not show any change with the annealing time, the BPDA-D polymer undergoes significant change in the glass transition region, as can be seen in Figure 7.

After 11 days of annealing, the tan δ decreases over the whole range of temperatures tested. Furthermore, the curve broadens and the two peaks are less pronounced, which is expected, as the content of the amorphous phase decreases with the increase in the crystalline fraction. This multiple-T_g relaxation behavior is characteristic for multiphase structures and incompatible blends. However, the behavior noticed in the BPDA-D polymer is peculiar because of the (consistently) reverse magnitudes of the two peaks (T_g(I), at the lower temperature and T_g(II), at the higher temperature). This can be expressed in terms of activation energies as well. Activation energies, E_a, are calculated from the Arrhenius plots (Figure S6, Supporting Information), as described in the Supporting Information. The peak at the lower temperature, T_g(I), exhibits higher E_a than the one at higher temperature, T_g(II) (see Table S1, Supporting Information). Such an observation can be explained by assuming a less mobile phase present at the crystal−amorphous phase interface.[47] Thus, based on the literature and the DSC evidence that the BPDA-D polymer is the only semicrystalline (Figure 6) polymer out of the four here investigated, we could explain the multiple tan δ peaks as follows: the relaxation occurring at about 33 °C is presumed to be the relaxation of the major part of the amorphous phase, a T_g per se. The relaxation occurring at a higher temperature of 46 °C can be attributed to the restricted amorphous phase located in the interfacial region.

The effect of the aromatic dianhydride architecture on the mechanical properties was also evaluated. Figure 8 shows

DOI: 10.1021/acssuschemeng.7b03026
ACS Sustainable Chem. Eng. 2018, 6, 668−678

representative strain−stress curves of the four PIs obtained at ambient temperature (T_{test} = 23 ± 2 °C). The mechanical performance changes significantly with varying the dianhydride architecture. ODPA-D polymer shows elastomeric behavior, which is as expected because its' T_g is below T_{test}, as opposed to the other three polymers that are in their glassy state ($T_g > T_{test}$).

The stress at break values (σ_b) increase in the order ODPA-D < BPADA-D < BPDA-D < 6FDA-D and the strain at break (ε_b) values in the following order BPADA-D < 6FDA-D < BPDA-D < ODPA-D. The 6FDA-D system shows the highest toughness and strain hardening while BPADA-D exhibits strain softening, having yield stress higher than its stress at break value. Young's moduli are in a broad range, from 90 MPa (ODPA-D) to 430 MPa (6FDA-D), comparable to the fatty acid dimer based polyamides of Hablot at al.[12] When compared to commercial fully aromatic PIs, these materials are roughly 1 order of magnitude lower in strength.[48]

The effect of annealing on the tensile properties is also shown in Figure 8. The three amorphous polymers (BPADA-D, ODPA-D, and 6FDA-D) show minor improvement of the mechanical properties with annealing time, while the effect on the semicrystalline BPDA-D is more evident. The stress at break value increases from 11 to 20 MPa, and the strain at break value decreases from 260% to 35%, despite the nonrelevant variation in T_g. The repeated fluorescence spectra after annealing the samples did not show any shifts in fluorescence peaks wavelengths.

CONCLUSIONS

A series of partially bio based semiaromatic polyimides varying in their aromatic dianhydride structure was synthesized in stoichiometric ratio with the fatty dimer diamine and their thermal, mechanical, and optical properties were investigated. The polymers obtained were fully organo-soluble thermoplastic branched polyimides with glass transition temperatures close to room temperature. Their solubility, amorphous thermoplasticity, and high thermal stability makes them easily processable and recyclable without deterioration of mechanical properties. The results have shown that the dianhydrides comprising a flexible ether spacer (BPADA and ODPA), as well as the one with rigid and bulky hexafluoroisopropylidene spacer (6FDA), yielded fully amorphous polymers. However, the dianhydride with no spacer (BPDA) provided a semicrystalline polymer structure with the annealing time, which lead to a constrained segmental relaxation. Despite their partially aliphatic and densely branched architectures, these polyimides were able to form the intermolecular charge transfer complexes, whose extent was dependent on the dianhydride electronic properties and evident from their fluorescence spectra and normalized dielectric loss. The increase in crystallinity with annealing time was shown to have a great effect on the tensile properties of the BPDA-D polymer despite no significant T_g variation was measured. The values of tan δ of these polymers (especially BPADA-D and 6FDA-D with values close to 2) were remarkably high over a broad range of near-room temperatures, which makes them great candidates in applications where high damping properties are required at ambiental conditions (noise or vibration insulating materials, shock absorbers, and sealants).

ASSOCIATED CONTENT

Supporting Information

The Supporting Information is available free of charge on the ACS Publications website at DOI: 10.1021/acssuschemeng.7b03026.

Additional characterization of all of the polymers from the main text. (PDF)

AUTHOR INFORMATION

Corresponding Author

*E-mail: a.susa@tudelft.nl.

ORCID

Arijana Susa: 0000-0002-3270-290X

Marianella Hernandez Santana: 0000-0002-0609-3485

Santiago J. Garcia: 0000-0002-2211-9972

Present Address

†Institute of Polymer Science and Technology (ICTP-CSIC), Juan de la Cierva, 3, 28006 Madrid, Spain.

Author Contributions

All authors contributed equally to this work.

Notes

The authors declare no competing financial interest.

ACKNOWLEDGMENTS

We thank Professor Sybrand van der Zwaag for his continued interest in the work and valuable comments on the manuscript during its construction. The authors acknowledge the financial support from the Dutch IOP program on self-healing materials under Grant No. IOP-SHM-012036. We acknowledge our industrial partner Croda Nederland BV, especially the sustained support and valuable discussions with Dr. Angela Smits (Croda). Many thanks to Dr. Brian Richard Pauw (Bundesanstalt für Materialforschung und−prüfung, Berlin) for performing the SAXS measurements.

REFERENCES

(1) Williams, C. K.; Hillmyer, M. A. Polymers from Renewable Resources: A Perspective for a Special Issue of Polymer Reviews. *Polym. Rev.* **2008**, *48* (1), 1−10.

(2) Bozell, J. J. Feedstocks for the Future − Biorefinery Production of Chemicals from Renewable Carbon. *Clean: Soil, Air, Water* **2008**, *36* (8), 641−647.

(3) Adekunle, K. F. A Review of Vegetable Oil-Based Polymers: Synthesis and Applications. *Open J. Polym. Chem.* **2015**, *05* (03), 34−40.

(4) Jain, J. P.; Sokolsky, M.; Kumar, N.; Domb, A. J. Fatty Acid Based Biodegradable Polymer. *Polym. Rev.* **2008**, *48* (1), 156−191.

(5) Miao, S.; Wang, P.; Su, Z.; Zhang, S. Vegetable-Oil-Based Polymers as Future Polymeric Biomaterials. *Acta Biomater.* **2014**, *10* (4), 1692−1704.

(6) Xia, Y.; Larock, R. C. Vegetable Oil-Based Polymeric Materials: Synthesis, Properties and Applications. *Green Chem.* **2010**, *12* (11), 1893−1909.

(7) Meier, M. A.; Metzger, J. O.; Schubert, U. S. Plant Oil Renewable Resources as Green Alternatives in Polymer Science. *Chem. Soc. Rev.* **2007**, *36* (11), 1788−1802.

(8) Maisonneuve, L.; Lebarbe, T.; Grau, E.; Cramail, H. Structure-Properties Relationship of Fatty Acid-Based Thermoplastics as Synthetic Polymer Mimics. *Polym. Chem.* **2013**, *4* (22), 5472−5517.

(9) Cordier, P.; Tournilhac, F.; Soulie-Ziakovic, C.; Leibler, L. Self-Healing and Thermoreversible Rubber from Supramolecular Assembly. *Nature* **2008**, *451* (7181), 977−980.

(10) Aboudzadeh, A.; Fernandez, M.; Muñoz, M. E.; Santamaría, A.; Mecerreyes, D. Ionic Supramolecular Networks Fully Based on Chemicals Coming from Renewable Sources. *Macromol. Rapid Commun.* **2014**, *35* (4), 460−465.
(11) Lutz, A.; van den Berg, O.; Van Damme, J.; Verheyen, K.; Bauters, E.; De Graeve, I.; Du Prez, F. E.; Terryn, H. A Shape-Recovery Polymer Coating for the Corrosion Protection of Metallic Surfaces. *ACS Appl. Mater. Interfaces* **2015**, *7* (1), 175−183.
(12) Hablot, E.; Donnio, B.; Bouquey, M.; Avérous, L. Dimer Acid-Based Thermoplastic Bio-Polyamides: Reaction Kinetics, Properties and Structure. *Polymer* **2010**, *51* (25), 5895−5902.
(13) van Velthoven, J. L. J.; Gootjes, L.; Noordover, B. A. J.; Meuldijk, J. Bio-Based, Amorphous Polyamides with Tunable Thermal Properties. *Eur. Polym. J.* **2015**, *66*, 57−66.
(14) Boumbimba, R. M.; Wang, K.; Hablot, E.; Bahlouli, N.; Ahzi, S.; Avérous, L. Renewable Biocomposites Based on Cellulose Fibers and Dimer Fatty Acid Polyamide: Experiments and Modeling of the Stress−Strain Behavior. *Polym. Eng. Sci.* **2017**, *57* (1), 95−104.
(15) Reulier, M.; Boumbimba, R. M.; Walsh Korb, Z.; Vaudemont, R.; Avérous, L. Thermomechanical and Cyclic Behavior of Biocomposites Based on Renewable Thermoplastics from Dimer Fatty Acids. *J. Appl. Polym. Sci.* **2017**, *134* (12), 44610.
(16) Susa, A.; Bose, R. K.; Grande, A. M.; van der Zwaag, S.; Garcia, S. J. Effect of the Dianhydride/Branched Diamine Ratio on the Architecture and Room Temperature Healing Behavior of Polyetherimides. *ACS Appl. Mater. Interfaces* **2016**, *8* (49), 34068−34079.
(17) van der Kooij, H. M.; Susa, A.; García, S. J.; van der Zwaag, S.; Sprakel, J. Imaging the Molecular Motions of Autonomous Repair in a Self-Healing Polymer. *Adv. Mater.* **2017**, *29* (26), 1701017.
(18) Ando, S.; Matsuura, T.; Sasaki, S. Coloration of Aromatic Polyimides and Electronic Properties of Their Source Materials. *Polym. J.* **1997**, *29* (1), 69−76.
(19) Ayala, D.; Lozano, A. E.; De Abajo, J.; De La Campa, J. G. Synthesis and Characterization of Novel Polyimides with Bulky Pendant Groups. *J. Polym. Sci., Part A: Polym. Chem.* **1999**, *37*, 805−814.
(20) Hegde, M.; Shahid, S.; Norder, B.; Dingemans, T. J.; Nijmeijer, K. Gas Transport in Metal Organic Framework−Polyetherimide Mixed Matrix Membranes: The Role of the Polyetherimide Backbone Structure. *Polymer* **2015**, *81*, 87−98.
(21) Ogieglo, W.; Madzarevic, Z. P.; Raaijmakers, M. J. T.; Dingemans, T. J.; Benes, N. E. High-Pressure Sorption of Carbon Dioxide and Methane in All-Aromatic Poly(etherimide)-Based Membranes. *J. Polym. Sci., Part B: Polym. Phys.* **2016**, *54* (10), 986−993.
(22) Ragosta, G.; Abbate, M.; Musto, P.; Scarinzi, G. Effect of the Chemical Structure of Aromatic Polyimides on Their Thermal Aging, Relaxation Behavior and Mechanical Properties. *J. Mater. Sci.* **2012**, *47* (6), 2637−2647.
(23) Li, F.; Ge, J. J.; Honigfort, P. S.; Fang, S.; Chen, J.-C.; Harris, F. W.; Cheng, S. Z. D. Dianhydride Architectural Effects on the Relaxation Behaviors and Thermal and Optical Properties of Organo-Soluble Aromatic Polyimide Films. *Polymer* **1999**, *40* (18), 4987−5002.
(24) McCreight, K. W.; Ge, J. J.; Guo, M.; Mann, I.; Li, F.; Shen, Z.; Jin, X.; Harris, F. W.; Cheng, S. Z. D. Phase Structures and Transition Behaviors in Polymers Containing Rigid Rodlike Backbones with Flexible Side Chains. V. Methylene Side-Chain Effects on Structure and Molecular Motion in a Series of Polyimides. *J. Polym. Sci., Part B: Polym. Phys.* **1999**, *37* (14), 1633−1646.
(25) Wood-Adams, P.; Costeux, S. Thermorheological Behavior of Polyethylene: Effects of Microstructure and Long Chain Branching. *Macromolecules* **2001**, *34* (18), 6281−6290.
(26) Ghosh, A.; Mistri, E. A.; Banerjee, S. Fluorinated Polyimides: Synthesis, Properties, and Applications. In *Handbook of Specialty Fluorinated Polymers*; Banerjee, S., Ed.; William Andrew Publishing: Amsterdam, 2015; pp 97−185.
(27) Acar, H. Y.; Ostrowski, C.; Mathias, L. J. Investigation of Structure-Property Relationships in Aromatic Polyimides and Polyamides. In *Polyimides and Other High Temperature Polymers: Synthesis, Characterization and Applications*; Mittal, K. L., Ed.; VSP: Zeist, 2001; Vol. *1*, pp 3−18.
(28) Wakita, J.; Sekino, H.; Sakai, K.; Urano, Y.; Ando, S. Molecular Design, Synthesis, and Properties of Highly Fluorescent Polyimides. *J. Phys. Chem. B* **2009**, *113* (46), 15212−15224.
(29) Szczepanski, C. R.; Pfeifer, C. S.; Stansbury, J. W. A New Approach to Network Heterogeneity: Polymerization Induced Phase Separation in Photo-Initiated, Free-Radical Methacrylic Systems. *Polymer* **2012**, *53* (21), 4694−4701.
(30) Wu, C.-f.; Akiyama, S. Enhancement of Damping Performance of Polymers by Functional Small Molecules. *Chin. J. Polym. Sci.* **2002**, *20* (2), 119−127.
(31) Angell, C. A. Relaxation in Liquids, Polymers and Plastic Crystals — Strong/Fragile Patterns and Problems. *J. Non-Cryst. Solids* **1991**, *131*, 13−31.
(32) Schönhals, A.; Schlosser, E. Dielectric Relaxation in Polymeric Solids Part 1. A New Model for the Interpretation of the Shape of the Dielectric Relaxation Function. *Colloid Polym. Sci.* **1989**, *267* (2), 125−132.
(33) Schönhals, A. Molecular Dynamics in Polymer Model Systems. In *Broadband Dielectric Spectroscopy*; Kremer, F., Schönhals, A., Eds.; Springer-Verlag: Berlin, 2003; pp 248−251.
(34) Luo, M.-C.; Zhang, X.-K.; Zeng, J.; Gao, X.-X.; Huang, G.-S. Enhanced Relaxation Behavior below Glass Transition Temperature in Diene Elastomer with Heterogeneous Physical Network. *Polymer* **2016**, *91*, 81−88.
(35) Hasegawa, M.; Horie, K. Photophysics, Photochemistry, and Optical Properties of Polyimides. *Prog. Polym. Sci.* **2001**, *26* (2), 259−335.
(36) Tang, H.; Feng, H.; Luo, H.; Dong, L.; Feng, Z. The Aggregation State of Polyimide. *Eur. Polym. J.* **1997**, *33* (4), 519−523.
(37) Wachsman, E. D.; Frank, C. W. Effect of Cure History on the Morphology of Polyimide: Fluorescence Spectroscopy as a Method for Determining the Degree of Cure. *Polymer* **1988**, *29* (7), 1191−1197.
(38) Hasegawa, M.; Kochi, M.; Mita, I.; Yokota, R. Molecular Aggregation and Fluorescence Spectra of Aromatic Polyimides. *Eur. Polym. J.* **1989**, *25* (4), 349−354.
(39) Hasegawa, M.; Mita, I.; Kochi, M.; Yokota, R. Charge-Transfer Emission Spectra of Aromatic Polyimides. *J. Polym. Sci., Part C: Polym. Lett.* **1989**, *27* (8), 263−269.
(40) García, M. G.; Marchese, J.; Ochoa, N. A. Aliphatic−Aromatic Polyimide Blends for H2 Separation. *Int. J. Hydrogen Energy* **2010**, *35* (17), 8983−8992.
(41) Luo, L.; Yao, J.; Wang, X.; Li, K.; Huang, J.; Li, B.; Wang, H.; feng, Y.; Liu, X. The Evolution of Macromolecular Packing and Sudden Crystallization in Rigid-Rod Polyimide via Effect of Multiple H-Bonding on Charge Transfer (CT) Interactions. *Polymer* **2014**, *55* (16), 4258−4269.
(42) Yokoyama, H. Small Angle X-ray Scattering Studies of Nanocellular and Nanoporous Structures. *Polym. J.* **2013**, *45* (1), 3−9.
(43) Prosa, T. J.; Winokur, M. J.; McCullough, R. D. Evidence of a Novel Side Chain Structure in Regioregular Poly(3-alkylthiophenes). *Macromolecules* **1996**, *29* (10), 3654−3656.
(44) Pankaj, S.; Beiner, M. Confined Dynamics and Crystallization in Self-Assembled Alkyl Nanodomains. *J. Phys. Chem. B* **2010**, *114* (47), 15459−15465.
(45) Beiner, M.; Huth, H. Nanophase Separation and Hindered Glass Transition in Side-Chain Polymers. *Nat. Mater.* **2003**, *2* (9), 595−599.
(46) Arnold, F. E.; Bruno, K. R.; Shen, D.; Eashoo, M.; Lee, C. J.; Harris, F. W.; Cheng, S. Z. D. The Origin of β Relaxations in Segmented Rigid-Rod Polyimide and Copolyimide Films. *Polym. Eng. Sci.* **1993**, *33* (21), 1373−1380.
(47) Dechter, J. J.; Axelson, D. E.; Dekmezian, A.; Glotin, M.; Mandelkern, L. An Analysis of the β Transition of Linear and Branched Polyethylenes by Carbon-13 NMR. *J. Polym. Sci., Polym. Phys. Ed.* **1982**, *20* (4), 641−650.

DOI: 10.1021/acssuschemeng.7b03026
ACS Sustainable Chem. Eng. 2018, 6, 668−678

(48) Yu, X.; Liang, W.; Cao, J.; Wu, D. Mixed Rigid and Flexible Component Design for High-Performance Polyimide Films. *Polymers* **2017**, *9* (9), 451.

DOI: 10.1021/acssuschemeng.7b03026
ACS Sustainable Chem. Eng. 2018, 6, 668−678